Available online at www.sciencedirect.com
SCIENCE DIRECT®
Journal of Nuclear Materials 329–333 (2004) 347–351
journal of nuclear materials
www.elsevier.com/locate/jnucmat

TEM characterization of structure and composition of nanosized ODS particles in reduced activation ferritic–martensitic steels

M. Klimiankou, R. Lindau, A. Möslang *

Forschungszentrum Karlsruhe GmbH, Institut für Materialforschung I, P.O. Box 3640, 76021 Karlsruhe, Germany

Abstract

TEM investigations of different ODS steels were performed to gather information about the structure and composition of ODS particles. The structure of the nanometer-sized Y_2O_3 particles analysed by HRTEM shows a strong correlation of its crystallographic orientation with the alloy lattice. The orientation correlations $[1\,1\,0]_{YO}\|[1\,1\,1]_{FeCr}$ and $(1\,\bar{1}\,1)_{YO}\|(\bar{1}\,0\,1)_{FeCr}$ were found. HRTEM and energy-filtered transmission electron microscopy (EFTEM) investigations also show the formation of $Y_2Ti_2O_7$ ODS particles due to the addition of metallic Ti in the powder before MA. Argon gas used as inert gas during the mechanical alloying was detected and tiny Ar gas bubbles trapped at the surface of ODS particles were imaged in the steel by using EFTEM.

1. Introduction

Oxide dispersion strengthened (ODS) steels produced by mechanical alloying techniques have become increasingly interesting for structural applications in nuclear fission and fusion power plants during the past few years. For specific blanket and divertor applications a replacement of presently considered conventionally produced reduced-activation ferritic–martensitic (RAFM) steels by suitable ODS alloys would provide improved creep resistance at high temperatures and consequently increase the operating temperature in future fusion power reactors to approximately 650 °C or more. The attractiveness of high-strength, nanocomposited RAFM steels is not only due to favourable radiological properties, but also to a unique combination of small average grain sizes, high dislocation densities, and nanoclusters composed of Y–O and Y–O–Ti solute atoms, respectively.

Relevant mechanical properties, e.g. tensile strength, toughness, fatigue, and creep rupture of the alloy were screened recently within a wide temperature range, e.g. [1–3]. However, detailed information concerning the crystalline structure of the ODS particles, its orientation with respect to the alloy matrix, and the individual elementary composition is still lacking. This information is important for improving RAFM-ODS alloys by means of targeted nanostructural tailoring. The knowledge about ODS particles and their interaction with the matrix would also help to prove nanoscale theory and modelling with simulation approaches that will be designed specifically to address material structures and properties in the nanoscale regime. The experience shows that lattice coherency of the particles with surrounding matrix is of importance for strengthening and embrittlement mechanisms [4]. The present investigation analyses both structure and composition of Y–O and Y–Ti–O ODS particles embedded in typical RAFM-ODS alloys. In addition, direct proof of Ar-bubbles trapped at the surface of ODS particles will be presented. The origin of the bubbles and their possible impact on mechanical properties will be addressed.

* Corresponding author. Tel.: +49-7247 82 4029; fax: +49-7247 82 4567.
E-mail address: anton.moeslang@imf.fzk.de (A. Möslang).

0022-3115/$ - see front matter © 2004 Elsevier B.V. All rights reserved.
doi:10.1016/j.jnucmat.2004.04.083

2. Experimental

The RAFM-ODS alloys were produced by mechanical alloying (MA) of inert-gas-atomized master 7–9% CrWVTaTi steels together with 0.5 wt% yttria or with 0.5 wt% yttria/Ti powder. The nominal composition of both the steels is given in Table 1. Repeated impacts of energetic balls during MA resulted in a fairly homogeneous distribution of nanosized Y_2O_3 particles in the steel matrix. Mainly to keep the oxygen content as low as possible, argon gas was used as inert atmosphere during mechanical alloying. In a second step, the MA powders were consolidated at around 1050 °C by hot isostatic pressing (HIPing). To obtain a well-defined martensitic–ferritic structure, the investigated materials were finally subjected to a two-step heat treatment at temperatures between 980 and 1100 °C/30 min, followed by annealing at 750 °C/2 h.

The TEM samples were prepared using conventional electropolishing method with additional polishing by an ion milling system. This additional ion milling procedure is necessary for the correction of the inhomogeneous sample thickness which is mainly due to different precipitates. The transmission electron microscope (TEM) investigations were performed with an accelerating voltage of 200 kV using a FEI Tecnai 20 FEG microscope equipped with a Gatan Image Filter (GIF) for EFTEM measurements. A double tilt specimen holder was used for the exact orientation of the grains relative to the incident electron beam. The evaluation of high-resolution TEM (HRTEM) images was performed by means of fast Fourier transformation (FFT) of the images. The EFTEM investigations were performed using the three-windows method [5].

3. Results and discussion

3.1. Nanosized Y_2O_3 particles in RAFM alloys

The TEM investigations were performed on the material without Ti, with the composition given in Table 1 (heat 1). The crystallographic lattice of the metal matrix corresponds to α-Fe with a bcc structure and a lattice constant of $a_0 = 0.287$ nm [6]. Using the HRTEM it was possible to image the atomic planes of $\langle 1\,1\,0\rangle$ type. The Y_2O_3 powder material has a crystalline bcc structure with a 1.06 nm lattice constant [6]. The HRTEM investigations confirm this crystallographic structure also for the ODS particles embedded in the alloy. In addition, the HRTEM investigations reveal a strong correlation between the structure of the Y_2O_3 particles and the FeCr matrix. Fig. 1 shows the HRTEM image taken from an ODS particle which is surrounded by the matrix (M) lattice. This image was taken from the grain oriented with $[1\,1\,1]_M$ zone axis to the electron

Table 1
The nominal chemical composition of the ODS steels (wt%)

Element	C	Si	Mn	P	S	Ni	Cr	W	Ti	Y	O	N	Ar
Heat 1	0.11	0.05	0.40	<0.005	<0.005	0.005	9.0	1.10	0.01	0.30	0.21	0.03	–
Heat 2	0.13	0.005	<0.01	<0.001	0.003	0.01	8.85	1.94	0.20	0.27	0.17	0.01	0. 005

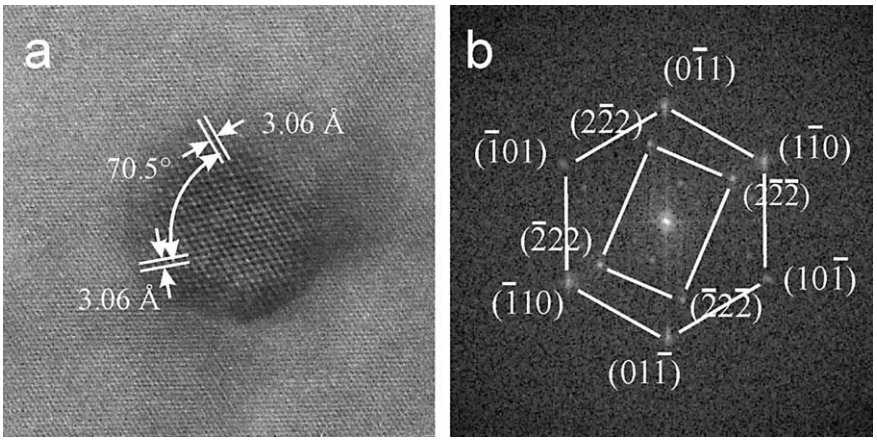

Fig. 1. HRTEM micrograph of the Y_2O_3 particle with surrounding matrix (a) and FFT image of this micrograph (b). The diffraction spots from Y_2O_3 particle of {2 2 2} type form the rectangle whereas diffraction spots from the matrix of {1 1 0} type form the marked hexagon at the [1 1 0] zone axis and [1 1 1] of matrix.

beam. The fast Fourier transformation (FFT) of the image shows the matrix lattice as a hexagonal pattern with diffraction spots of the {1 1 0} type and $d_{M(110)} = 0.203$ nm distance. In the FFT image, the Y_2O_3 (YO) lattice is rectangular with diffraction spots of the {2 2 2} type and corresponding atomic planes distance of $d_{YO(222)} = 0.306$ nm. The angle of 70.5° between diffraction spots of $\{2\,2\,2\}_{YO}$ type marked in Fig. 1(a) confirm that the Y_2O_3 particle is oriented with the [1 1 0] zone axis and, consequently, $[1\,1\,0]_{YO}\|[1\,1\,1]_M$. The orientation correlation of both lattices in the image plane is $(1\,\bar{1}\,\bar{1})_{YO}\|(1\,\bar{1}\,0)_M$. The angle between $[1\,\bar{1}\,1]_{YO}$ and $[0\,\bar{1}\,1]_M$ is 10.5°. This orientation relationship satisfies the Kurdjumov–Sachs relation [7]. There exist 24 possible variants of this relationship. Each orientation configuration will show its own diffraction pattern of the Y_2O_3 particle at the same matrix orientations. The diffraction pattern could appear like the ring of a polycrystalline sample, as the small volume ratio of the ODS particles in relation to the matrix does not allow a reliable imaging of its diffraction.

The Kurdjumov–Sachs relation is usually used for the description of the orientation relations in the bcc/fcc interfaces if both lattices have comparable lattice constants. The appearance of this relation in the Fe/Y_2O_3 system with bcc/bcc interface is possible due to the favourable epitaxial orientation of certain atomic planes in both materials. The parallel orientation between Fe(1 1 0) and Y_2O_3(1 1 1) directions has been confirmed on various small ODS-particles (diameter less than about 10–12 nm), and the consistency agreement of the atomic planes:

$$\frac{3d_{Fe(110)} - 2d_{Y_2O_3(222)}}{2d_{Y_2O_3(222)}} \approx 0.5\%$$

suggest that the epitaxial orientation of this atomic planes has its origin in a pronounced reorientation force. A more detailed HRTEM study of Y_2O_3 particles in the reduced activation EUROFER-ODS steel is described elsewhere [8].

3.2. Nanosized $Y_2Ti_2O_7$ in RAFM alloys

The separate addition of Ti powder and Y_2O_3 powder with a ratio of 1:1 during mechanical alloying (Table 1, heat 2) and subsequent hot pressing results in the formation of ultrafine ODS nanoparticles [9]. The TEM investigations of the present study confirm these observations in general. The bright field (BF) image (Fig. 2(a)) shows a typical example of the spatial distribution of nanosized ODS particles in the matrix. The images of the embedded ODS particles often have a contrast that is similar to that of the surrounding matrix on the TEM micrographs. They are visible as disks decorated at their perimeter. This decoration originates from Fresnel fringes at the boundaries between two phases in the under-focus adjustment. Numerous ODS particles have two or even three closely located bright areas which are much smaller than the ODS particles. The contrast of these bright areas is similar to the matrix contrast observed on the exactly focused TEM image. The bright contrast on the under-focused image indicates that those parts are cavities or bubbles in the material [10].

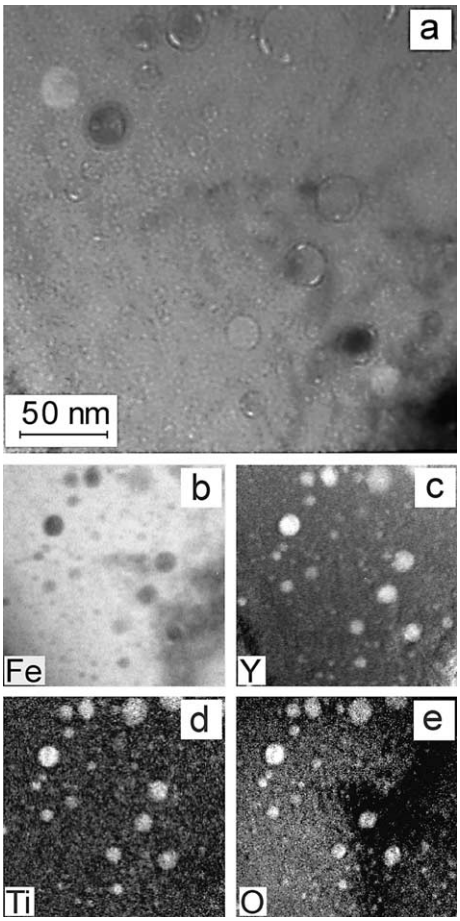

Fig. 2. Conventional bright field (a) and EFTEM images (b)–(e) of $Y_2Ti_2O_7$ ODS particles in reduced-activation ferritic–martensitic steel. The bright field image were taken slightly defocused in order to enhance the particle contrast. The EFTEM mapping images were acquired using Fe $L_{2,3}$, Y $M_{5,6}$, Ti $L_{2,3}$, and O K EELS edges.

The resulting energy-filtered images are presented in Fig. 2(b)–(e). The dark regions on the Fe $L_{2,3}$ image (Fig. 2(b)) show the local Fe deficiency. The image gives a clear view of all kinds of precipitates and particles in the matrix. Also the signal-to-noise ratio is better than on the bright field image and thus allows the detection of small ODS particles which are not visible on the BF image. The other three images (Fig. 2(c)–(e)) acquired by the filtering of the Y $M_{4,5}$, Ti $L_{2,3}$, and O K edges exhibit

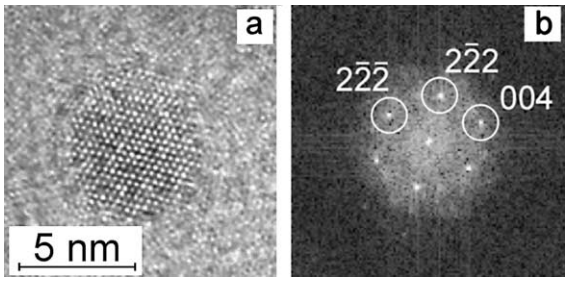

Fig. 3. HRTEM micrograph of a $Y_2Ti_2O_7$ particle (a) and FFT image of this micrograph (b). The diffraction spots from $Y_2Ti_2O_7$ particle of {2 2 2} and {0 0 4} types are marked with circles.

the same pattern of the bright spots which correspond to the ODS particles observed on the BF and Fe images. This suggests that all ODS particles have the same Y–Ti–O composition. No formation of pure Y–O particles was observed. The most important advantage of the EFTEM method compared to the conventional TEM is the determination of spatial elemental distribution over large areas, even if these elements do not produce sufficient contrast in the conventional TEM images.

There exist six different Y–Ti–O compositions with different stoichiometry and crystallographic structures [6]. The exact identification of the chemical phases of ODS particles was performed by using HRTEM methods. Fig. 3(a) shows a HRTEM micrograph from an ODS particle in which two atomic planes are visible simultaneously. A combination of the interplanar distances and the angle between the systems of planes is given in Fig. 3(b) for the (0 0 4) and $(2\bar{2}2)$ atomic planes of $Y_2Ti_2O_7$ cubic ($a_0 = 1.01$ nm) phases with the [1 1 0] zone axis. Actually, the measured data are equal to the following data calculated from the $Y_2Ti_2O_7$ structure: $d_{222} = 0.29$ nm, and $d_{004} = 0.25$ and the angle between $(2\bar{2}2)$ and (0 0 4) atomic planes of 54.7°. The analysis of HRTEM picture combined with EFTEM results show definitely that ODS particles have $Y_2Ti_2O_7$ composition.

3.3. Ar-bubbles trapped at ODS particles

As was mentioned above, a significant number of ODS particles is decorated by cavities (Fig. 2(a)). The EFTEM investigation of the elemental composition of an ODS particle with two cavities is presented in Fig. 4. The cavities are marked by arrows and reflected on the bright field micrograph (Fig. 4(a)). The large cavity is 15 nm long and 9 nm wide. The second flat cavity is 9 nm long and only 3 nm wide. EFTEM images presented in Fig. 4(b)–(f) have been prepared using the respective elemental EEL edge. The contrast of the images reflects the spatial distribution of the element investigated. The signal from the Fe $L_{2,3}$ edge becomes

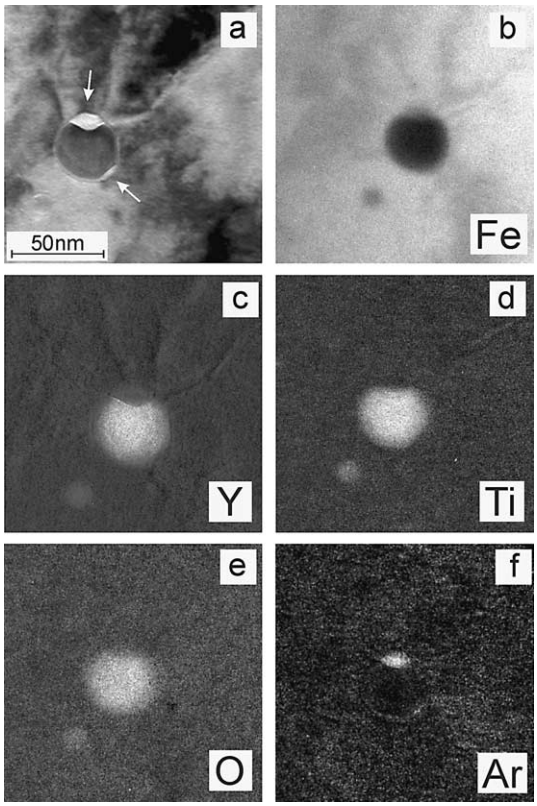

Fig. 4. EFTEM micrographs taken from one ODS particle using the three windows method: (a) presents the bright field image, whereas the images using the Fe $L_{3,2}$, Y $M_{5,4}$, Ti $L_{3,2}$, O K, and Ar $L_{3,2}$ edges are presented in (b)–(f), respectively.

weaker at the location of the ODS particle and cavity (Fig. 4(b)). This confirms its location inside the matrix. The energy-filtered images presented in Fig. 4(c)–(e) were taken at the edges of Ti $L_{2,3}$, O K, and Y $M_{4,5}$. The element distribution shown by the images corresponds to that of a $Ti_2Y_2O_7$ particle composition. Also the smaller ODS particle in the vicinity of the larger ODS particle, which is not clearly visible in the bright field image, is clearly reflected by the filtered images. Its elemental composition corresponds to the composition of the larger particle. The additional EFTEM image taken using the Ar $L_{2,3}$ edge clearly shows the presence of Ar inside the 'big' cavity, whereas the question concerning the presence of Ar gas inside the small cavity at the opposite side of the ODS particle cannot be definitely answered (Fig. 4(f)).

Although the observed nanocavities filled with Ar gas only have a minor influence on swelling, as its estimated total volume ranges from 0.03% to 0.1%, worldwide experience with implantation or irradiation induced helium has shown that even small concentrations in the range of some tens of appm can lead to ductility reduction or dynamic fracture toughness degradation. In

addition, annealing experiments of irradiation induced He-bubbles beyond the $\alpha \rightarrow \gamma$ transition temperature (780–820 °C in the present steels) lead to bubble migration and coalescence with relatively large and stable He gas filled cavities as end product that certainly cause problems for any subsequent joining treatments. Therefore it is suggested to replace the argon atmosphere during the mechanical alloying by a more appropriate one.

4. Conclusion

HRTEM investigations of oxide dispersion strengthened RAFM steel clearly revealed the existence and origin of an unexpectedly strong orientation correlation between nanoscale Y_2O_3 particles and the surrounding alloy matrix. The orientation correlation was found to be $[1\,1\,0]_{YO} \| [1\,1\,1]_M$ and $(1\,\bar{1}\,\bar{1})_{YO} \| (1\,\bar{1}\,0)_M$. The EFTEM investigations performed on the RAFM alloys with Y_2O_3 and $Y_2Ti_2O_7$ ODS particles show the spatial homogeneous distribution of the particles as well as the composition. The HRTEM measurements show that ODS particles in the RAFM alloys with Ti addition have $Y_2Ti_2O_7$ composition. For the first time, nanosized cavities were found to be formed during Hipping processes by the Ar gas which was incorporated into the material during mechanical alloying. The cavity are preferably trapped at the surface of ODS particles. The Ar bubbles were imaged by using EFTEM mapping of the Ar $L_{3,2}$ edge. As argon bubbles trapped at the surface of ODS particles and/or precipitates are expected to have a negative impact both on some mechanical properties and on any joining treatments, it is suggested to replace the argon atmosphere during mechanical alloying.

References

[1] R. Lindau, A. Möslang, M. Schirra, P. Schlossmacher, M. Klimenkov, J. Nucl. Mater. 307 (2002) 769.
[2] S. Ukai, M. Fujiwara, J. Nucl. Mater. 307–311 (2002) 749.
[3] B.A. Pint, I.G. Wright, J. Nucl. Mater. 307–311 (2002) 763.
[4] S.S. Campos, E.V. Morales, H.-J. Kestenbach, Metall. Mater. Trans. A 32 (2001) 1245.
[5] L. Reimer (Ed.), Transmission Electron Microscopy, Springer Series in Optical Science 36, Springer, Berlin, 1997, p. 452.
[6] J.V. Smith, American Society for Testing Materials, Powder diffraction file, 13. Inorganic, Philadelphia, PA, 1962–1965.
[7] C.P. Luo, U. Dahmen, Acta Mater. 46 (1998) 2063.
[8] M. Klimiankou, R. Lindau, A. Möslang, J. Cryst. Growth 249 (2003) 381.
[9] V.V. Sagaradze, V.I. Shalaev, V.L. Arbuzov, B.N. Goshchitskii, Y. Tian, W. Qun, S. Jiguang, J. Nucl. Mater. 295 (2001) 265.
[10] B.L. Eyre, in: R.e. Batist, J. Nihoul, L. Stals (Eds.), Proceedings of the International Discussion Meeting 20–22 SCK/CEN MOL, 1971, p. 311.